The International Journal of Advanced Manufacturing Technology (2020) 106:3239–3251
https://doi.org/10.1007/s00170-019-04688-w

ORIGINAL ARTICLE

Accurate model construction of deformed aero-engine blades for remanufacturing

Cheng Su[1,2] · Xin Jiang[1,3,4] · Guanying Huo[1,3,4] · Qiang Zou[2] · Zhiming Zheng[1] · Hsi-Yung Feng[2]

Received: 26 June 2019 / Accepted: 10 November 2019 / Published online: 4 January 2020

Abstract

Remanufacturing for aero-engine blades is an essential operation in current aerospace maintenance industry due to the significant cost savings involved. However, the individual geometric deformation in the damaged blades makes it very difficult to repair them automatically due to the lack of a model for the deformed blade. This paper proposes a new method to adaptively construct an accurate deformed blade model for remanufacturing by finding the deformation rule between the nominal blade model and the measured data collected from the deformed blade via scanning. Considering the precision of the scanned data, the flat regions of the scanned data and nominal model (suction face and pressure face) are segmented and extracted first. To achieve accurate matching results, the segmented scanned data are matched with the segmented nominal model by maintaining local rigidity under the optimal ICP (iterative closest point) framework. Then, the nonflat regions of the nominal model (leading edge and trailing edge as well as the damaged region) are stitched with the scanned data at selected fixed locations to construct the deformed blade model. A twisted compressor blade with some tip damage was selected in the case study to demonstrate the effectiveness of the proposed method. A reference deformed blade model acquired by a computational fluid dynamics software tool was utilized for comparison, and machining simulation was carried out to verify the remanufacturing result.

Keywords Aero-engine blade · Remanufacture · Deformation · Accuracy

1 Introduction

Aero-engine blades, such as turbine and compressor blades, take the central place in the modern aerospace industry. Working in the environment with very high temperature and pressure as well as being impacted with foreign objects, aero-engine blades may suffer from many kinds of damages, such as wear, corrosion, and fatigue [1, 2]. To survive in such a harsh environment, blades are usually made of titanium- or nickel-based alloys which are extremely rare and difficult to machine. Taking the economy cost into consideration, extending the service life of blades via remanufacturing is an inevitable choice since replacing with a new one is far more expensive.

Generally, the damaged blade remanufacturing process mainly involves the following stages: pre-inspection, build-up, removal, and post-inspection, as shown in Fig. 1. On pre- and post-inspection aspects, contact or noncontact measurement instruments are utilized to digitize the damaged/deposited/repaired blades, and the microstructure of repaired blades has to be evaluated. In the build-up process, welding or laser cladding is employed to fill up the missing volume of the damaged part. However, the current build-up techniques cannot restore the damaged blade accurately. Excess material in the raw deposited blade has to be removed by NC machining/grinding and polishing to meet the requirements of geometric size and surface smoothness. Until the early twenty-first century, most stages of the blade repair process had been carried out manually which is time-consuming and labor-intensive. Besides, the repair quality entirely relies on the operators' individual experience, and the repair results

✉ Xin Jiang
jiangxin@buaa.edu.cn

✉ Guanying Huo
gyhuo@buaa.edu.cn

[1] LMIB and School of Mathematics and Systems Science, Beihang University, Beijing 100191, China

[2] Department of Mechanical Engineering, The University of British Columbia, Vancouver, BC V6T 1Z4, Canada

[3] Beijing Advanced Innovation Center for Big Data and Brain Computing, Beihang University, Beijing 100191, China

[4] Peng Cheng Laboratory, Shenzhen 518055, Guangdong, China

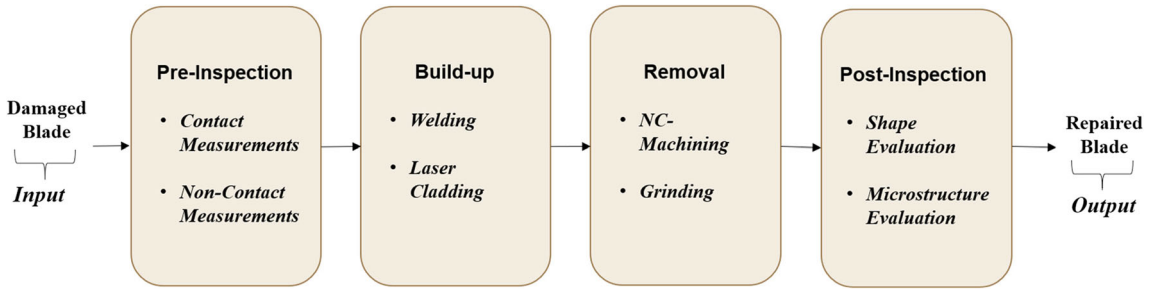

Fig. 1 Blade repair process

differ from each other due to the lack of a precise geometric description of the damaged region. To reduce the labor and time costs as well as to enhance repair reliability, some efforts have been made to automate scanning [3–6], laser cladding [7–10], and machining process [11, 12]. Furthermore, integrating these stages [8, 12–15] became both the research and industry interests due to fewer costs and higher efficiency.

In the automated and adaptive blade repair process, target model construction for remanufacturing always takes the key position, because the tool paths for laser cladding and machining are directly generated based on this model. The aerodynamic performance of blades requires a smooth geometric transition on the blade surface. After NC machining stages, there are still some surface discontinuities between the deposited section and the undamaged section which forms a visible interface. The remanufacturing efficiency benefits from a more accurate model as less post-processing work needs to be carried out, such as polishing. However, due to the extreme working conditions, the shapes of aero-engine blades deform to different degrees. The nominal model (original CAD) is obviously inappropriate to utilize for repairing. For the past 20 years, reverse-engineering-based methods [9, 12, 14–17] and design-feature-based methods [18–21], as two main strategies for blade repairing, have been developed. The reverse-engineering-based methods attempt to restore damaged blade geometry via the measured data and reverse-engineering tools [9, 12, 14–16]. Since the measured data of the damaged part is not reliable, the restored geometry loses accuracy. The design-feature-based methods try to keep some design features or intents in several blade cross-sections by fitting the measure data [19, 21]. However, it is difficult to accurately determine the cross-sections in the measured data, and cross-section geometry cannot be utilized in the blade tip repairing. How to construct an intact deformed blade model accurately is a challenging task since only measured data of the undamaged section are available and reliable.

To guarantee successful damaged blade remanufacturing, the accuracy of the deformed blade model is the focus of our attention. A novel approach based on the accurate matching of measured data and nominal CAD through keeping local rigidity is proposed in this paper. Considering that 3D optical scan only accurately works on a flat area [16], the matching process is performed on the segmented flat surfaces. The profile of the blade consists of two sharp edges: leading edge (LE) and trailing edge (TE), and two surfaces: suction face (SF) and pressure face (PF). Many measured noises and outliers may exist on the LE and TE as well as raw deposited part via 3D optical scanning. Therefore, the undamaged part of the SF and PF in the measured data is segmented and matched with the nominal CAD. Then, the rest of the parts will be stitched up with the matched part with least shrinkage or expansion to form the intact deformed model. In implementation, the input data which is simulated as the deformed blade is achieved by fluid–structure coupling calculation via ANSYS CFX for comparing and verifying. We demonstrate the applicability of our method in two ways: the comparison of the constructed blade model and the deformed blade data, and the machining simulation result.

2 Existing blade model creation methods

Constructing a deformed blade model is vital in the whole manufacturing or repairing process. Common failure types [2] including impact damage from foreign objects, wear of the blade, cracks, corrosion, etc. occur on different blade regions. Many valuable works have been devoted for the deformed blade model construction of different damaged regions, such as the blade tip [8, 12, 14], blade edge [10, 16], and blade profile surface [19, 21]. According to the design information or knowledge being taken into consideration as an additional input in the model construction process, existing methods can be roughly classified into two categories: RE-based methods and design-feature-based methods.

2.1 Reverse-engineering-based methods

RE technologies are aimed at creating a virtual CAD model for an existing component based on 3D measured point data. Therefore, RE-based methods have become the first choice for

carrying out the blade remanufacturing/repairing for most people. Gao et al. [16] presented an adaptive detect-free polygon modeling approach through RE tools. Using the Bezier surface to fill the holes caused by the digitizing process or defect deletion, an intact polygon model was created for comparing with the actual scanning data and extracting a repair patch for welding and machining.

For creating a nominal model of worn aerospace components, the geometry of straight and curved blades was analyzed by Gao et al. [14]. Then the reconstructing procedure about how to extrapolate and extend the blade surface for tip repair through reverse-engineering software of PolyWorks was introduced. Similarly, Bagci [17] described the model construction steps for recovery of broken or worn parts using Pro/Engineer CAD/CAE/CAM software, Yilmaz et al. [12] developed an adaptive RE reconstruction method for remodeling of deposited blade through Rhinoceros 3D modeling package, and Wilson et al. [9] demonstrated a semi-automated geometric reconstruction in CATIA software which constructed a solid model by running prominent cross-section (PCS) algorithm in a nondefective region and extrapolating over the remaining height of the defective blade. Li et al. [15] also adopted the combinational method of PCS and extrapolation to reconstruct the nominal model, then a modified ICP algorithm was proposed for the fine registration.

RE-based methods are only relying on the scanned data to restore the damaged blade model. However, there are some common difficulties or problems when carrying out RE-based methods. Firstly, RE-based methods depend on the measured points data, but the geometric information about the defects has been damaged or missing. Extrapolation and extension are adopted in most cases, which only keep the smooth transition rather than the accuracy, especially for twisted/curved blades. Secondly, there are many manual interventions such as the recognition and deletion of the unconspicuous defects when constructing the CAD model for building-up or machining. Besides, the operation procedure of the RE tool is complex and time-consuming.

2.2 Design-feature-based methods

Different from the RE-based methods, the design information or knowledge is introduced to construct a more accurate blade model. Design-feature-based methods generate a valid blade model by capturing and keeping some important design features during the reverse-engineering process.

The nominal model or unused blade scanned data, which is called the master model, is one of the most direct and easy-to-use design features. Zheng et al. [22] presented a method for repairing worn-out turbine blades by laser welding and cladding automatically. After a point-to-surface best-fitting operation, the worn area was recognized and extracted by comparing the distance between scanned point clouds and nominal CAD with the predefined tolerance, then a triangle mesh model representation for the damaged area was generated and transferred into STL file. Based on the additive manufacture technique, Zhang et al. [10] presented an automated damage detection and reconstruction algorithm by fitting the reconstructed model with the nominal model and comparing the overlapping area of each corresponding slice. However, the deformation of damaged blades caused by long-lasting working in the harsh environment was not taken into consideration, which results in the obvious deviation between the reconstructed model and measured data. We cannot achieve the accurate model for the deformed blades just through the master model.

In order to obtain a more accurate result, the design intents have been introduced into deformed model reconstruction. Assuming that the tip will have the same tendency of distortion as the lower section of the blade, Ng et al. [18] built the relationship between the profile of the master model and the profiles of the worn blade under each layer by introducing the neutral line concept and adopting the interpretation vector method in order to reconstruct a profile geometry of the damaged turbine blade. Mohaghegh et al. [19] suggested that seven circular arcs on section profiles as a design key point can lead to a valid shape of the blade, then they constructed the geometry model of a turbine blade using the segmentation and constrained fitting algorithm. As an improved work, Mohaghegh et al. [20] incorporated the design intents and construction geometry behind a sample heavy-duty turbine blade during reverse engineering. Reference sections, stacking axis, and blade twist, which depict the shape of the blade from 2D to 3D, were analyzed to restore the blade surface. Considering deformation caused by long-lasting working, Rong et al. [21] transformed the template curves of the design CAD model to achieve the best fit to measured points on several 2D cross-sectional profiles. Based on the aforementioned design concepts and intents, the shape of 2D cross-sectional profiles should be restored firstly. However, the cross-section geometry of the blade tip is damaged and cannot be utilized in the blade tip repairing. Besides, it is not accurate enough to depict the deformed blade geometry by fitting several cross-sectional profiles. To construct an accurate model of the deformed blade, we argue that the whole 3D blade model should be directly employed instead of the discrete 2D cross-section layers.

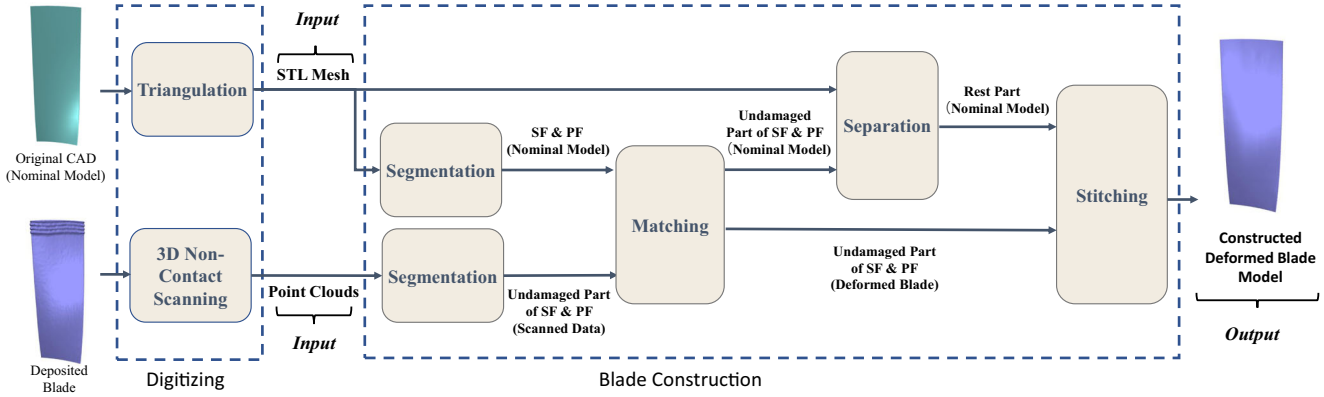

Fig. 2 Overview of the proposed method

3 Methodology

3.1 Overview

The proposed method aims at constructing an accurate model of the deformed blades based on the measured data points and guidance of the nominal model for remanufacturing. The flowchart of our method is shown in Fig. 2. Different from the methods that use several sampled 2D cross-sectional profiles of the blade, the nominal model is brought in as a whole for maintaining the entire geometry and mesh topology. Except the triangulation of the nominal model, the measured data of the deposited blade is the other input of our algorithm. The build-up process is not involved in the proposed method.

Due to the noises and outliers which are usually gathering at the sharp area such as the LE and TE, the segmentation is carried out firstly in both inputs to avoid interference by applying a region growing algorithm constrained with the smoothness and curvature. Then the SF and PF of the nominal model and the undamaged part of the SF and PF of scanned data are extracted. An optimal ICP framework with the local rigidity amendment is developed to acquire an accurate matching result by avoiding the shrink and expansion. The separation will divide the nominal model into the undamaged part of SF and PF which is corresponding to the undamaged part of SF and PF of the deformed blade and the rest of the parts of the nominal model which include the LE, TE, and the damaged region. Lastly, the constructed deformed blade model is obtained by stitching the nominal model to some fixed positions of the deformed blade under the constraints of keeping the local rigidity as much as possible.

3.2 Segmentation

Noises and outliers during 3D noncontact measurement are almost unavoidable because of the unexpected light disturbance, sharp edge/area, and invisible occluded regions [16]. Obviously, the measured data points with less error result in the more accurate deformed blade model. The blade surface consists of the SF, PF, LE, and TE, in which noises and outliers often appear on LE and TE since the 3D scanner only works well on a flat area. To avoid the interference of these unbearable errors in deformed blade model construction, the segmentation should be performed in both the nominal model and scanned data points of the deposited blade. Specifically, the segmentation is to distinguish two pairs of surface patches: one is the sharp edges and flat surfaces and the other one is the undamaged part and deposited part.

For the segmentation of the nominal model where only the flat patch should be distinguished from the sharp edge, the curvature properties of the surface are taken into consideration. Mean curvature which is defined as the average of the principal curvatures is tending to 0 on a flat surface, but is not on the leading edge and trailing edge. For the scanned data points of the deposited blade, the undamaged part of the PF and SF needs to be extracted. Obviously, the deposited region cannot meet the requirement of smoothness which shows a large change of mean curvature in the neighbor points. Therefore, the variance of the mean curvature of the neighbor points is used to scale the smoothness as follows:

$$S_i = \mathrm{Var}\{C_i\} = \frac{\sum_{j \epsilon \mathcal{N}_i} \left(C_j - C_i\right)^2}{n_i} \quad (1)$$

where p_j is the neighbor of p_i, C_i and C_j are the curvatures of points p_i and p_j, $\mathcal{N}_i$ is the neighbor point set of p_i, and n_i is the number of neighbor points of C_i.

Then each point/vertex is associated with two attributes: mean curvature and smoothness. A region growing algorithm constrained with these two attributes is adopted on the scanned data of the deposited blade to segment the

undamaged part, as shown in Algorithm 1. In this paper, the curvature and smoothness thresholds are set as 0.015 and $1.2e^{-4}$. In Figs. 3 and 4, we show the segmentation results of the nominal model and the scanned data, respectively.

Algorithm 1. Region Growing Segmentation

Input:

- Point cloud = $\{P\}$
- Points curvatures = $\{C\}$
- Points smoothness = $\{S\}$
- Seed point P_S
- Curvature threshold C_{th}
- Smoothness threshold S_{th}

Output:

- Region list $\{R\}$

Algorithm:

Region list $\{R\} \leftarrow \emptyset$

Available points list $\{A\} \leftarrow \{1, \ldots, |P|\}$

Current seeds $\{S_C\} \leftarrow P_S$

While $\{S_C\}$ is not empty **do**

  Current region $\{R_C\} \leftarrow \emptyset$

  $\{A\} \leftarrow \{A\} \setminus \{S_C\}$

  for $i = 1$ to **size**$(\{S_C\})$ **do**

    $\{N_C\} \leftarrow$ neighbors of current seed point $S_C\{i\}$

    $\{S_C\} \leftarrow \{S_C\} \setminus S_C\{i\}$

    for $j = 1$ to **size**$(\{N_C\})$ **do**

      Current neighbor point $P_j \leftarrow N_C\{j\}$

      if $\{A\}$ contains P_j and $C\{P_j\} < C_{th}$ and $S\{P_j\} < S_{th}$ **then**

        $\{R_C\} \leftarrow \{R_C\} \cup P_j$

        $\{A\} \leftarrow \{A\} \setminus P_j$

        $\{S_C\} \leftarrow \{S_C\} \cup P_j$

      end if

    end for

  end for

  Add current region to global segment list $\{R\} \leftarrow \{R\} \cup \{R_C\}$

end while

Return $\{R\}$

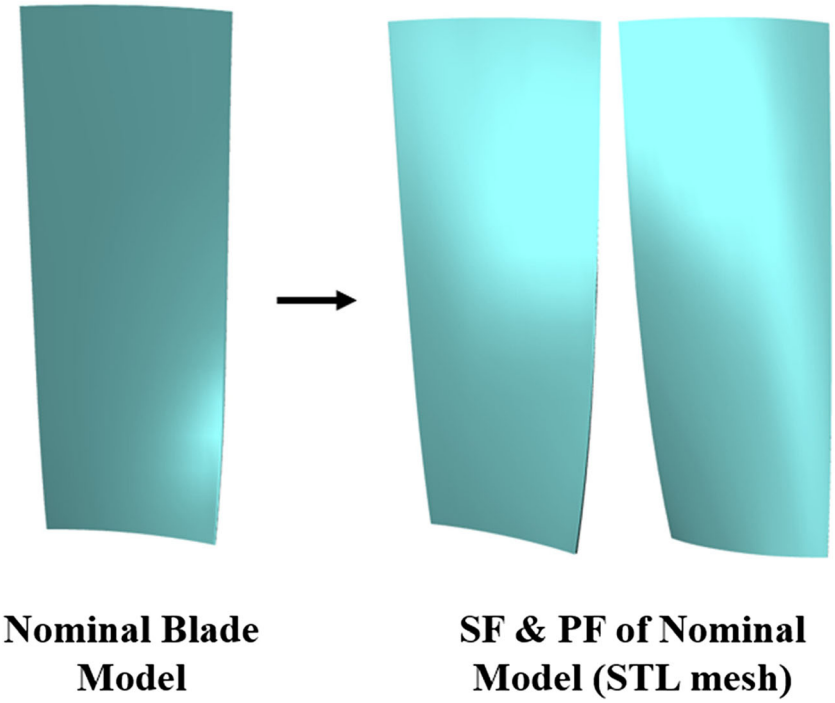

Fig. 3 Segmentation of the nominal blade model

3.3 Matching

To construct the deformed blade model, we try to find out the rule of blade deformation based on the segmented surfaces of the nominal model and scanned data. The matching is to construct the relationship between a template surface and a target surface. There is always a point in the nominal CAD corresponding to the selected point of segmented scanned data, but not vice versa, because the scanned data of the deposited region has already been deleted in the segmentation. Regarding the segmented nominal model as the target surface in which every template point, the segmented scanned point, has its correspondence, we find out the mapping from the template to the target. Then the reverse mapping brings the corresponding nominal model data to the best alignment with the scanned data. As shown in Fig. 5, the matching is operated as the following three main steps: initial matching, target surface projecting, and local rigidity keeping. We put the steps of target surface projecting and local rigidity keeping into the iterative loop to achieve an accurate matching result.

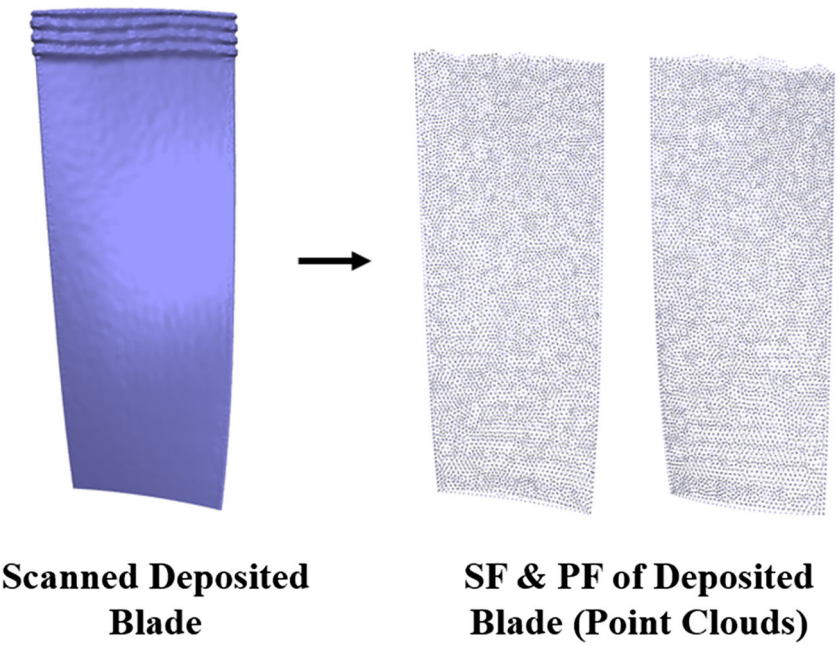

Fig. 4 Segmentation of scanned data of the deposited blade

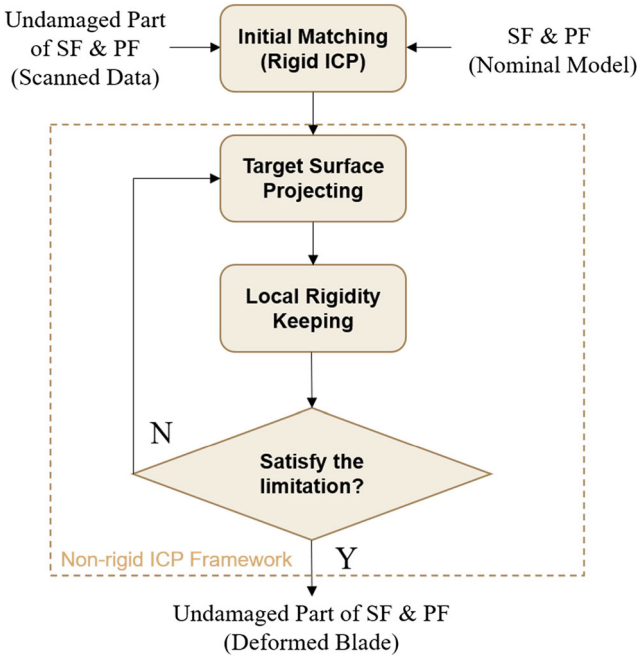

Fig. 5 Matching process

These following steps constitute the basic framework of the iterative closest point (ICP) algorithm:

Select some points **P** from the template surface.
Search for the closest points **Q** in the target surface.
Minimize the cost function of selected points and their closest points, and obtain the transformation(s).
Update the selected points **P** according to the transformation(s).
Calculate the average distance between the template points **P** and target points **Q**.
If the average distance is less than a predefined threshold or the number of iterations is larger than the set number, stop the algorithm and return. Else, back to step 2 and start next iteration.

3.3.1 Initial matching

The rigid ICP method is used for initial matching to make the segmented scanned data coincide roughly with the SF and PF of the nominal model. This rigid transformation can be divided into rotation and translation, both of which have three degrees of freedom. Generally, the cost function expressed by the term of the sum of squared errors is utilized to measure the result of matching as follows:

$$E = \sum_{i=1}^{N} \|\tau(p_i) - q_i\|^2 \tag{2}$$

where $\mathbf{P} = \{p_1, p_2, p_3, \ldots, p_N\}$ is the selected point set from the scanned data and $\mathbf{Q} = \{q_1, q_2, q_3, \ldots, q_N\}$ is the corresponding point set from target surface S_{target}, τ is the decision variable of this least square problem which can be divided into a rotation matrix **R** and a translation **T** as $\tau(p_i) = \mathbf{R} \cdot p_i + \mathbf{T}$.

In these ICP methods, the selection of correspondences, which refer to the searching range in the template surface, is vital for the matching result. In our case, the deformation between the nominal model and the scanned data reduces the accuracy of matching, and the great number of data points increases the computational complexity. To solve the above two problems, the searching range of correspondences in the first iteration can be limited to the points on the blade root which suffers from the minimum deformation and can be recognized easily.

3.3.2 Target surface projecting

In the target surface projecting, the error metric about the deformed scanned data $\{D(p_i) | i = 1, 2, \ldots, N\}$ and the nominal model surface S_{target} is defined by the following cost function:

$$E_{\text{d}} = \sum_{i=1}^{N} \text{dist}^2(q_i, D(p_i)) \tag{3}$$

where $\text{dist}(q_i, D(p_i))$ is the distance between the deformed point $\mathcal{D}(p_i)$ and its closest points q_i on the nominal model surface S_{target}.

The nonrigid ICP algorithm [23, 24], which is employed to project the template onto the target surface, can be regarded as a deformation for the template surface and the appointed correspondences of the target surface. Different from the rigid ICP in which the same rigid transformation matrix is applied for all selected template points, the nonrigid ICP is to assign a transformation to each one under some imposed constraints. There are some common steps in performing the nonrigid ICP algorithm: finding out the nearest correspondences for every template point, calculating the transformations via minimizing the error metric, transforming the template points to new positions, and checking the threshold.

Assuming that the scanned data points set $\mathbf{P} = \{p_1, p_2, p_3, \ldots, p_N\}$ is given by the homogeneous coordinates $\overline{\boldsymbol{p_i}} = \left[x_{p_i}, y_{p_i}, z_{p_i}, 1\right]^T$, the deformation D can be expressed as a set of affine 3 × 4 transformations $D = \{\boldsymbol{D_1}, \boldsymbol{D_2}, \boldsymbol{D_3}, \ldots, \boldsymbol{D_N}\}$. Then the deformation of p_i can be written as $D(p_i) = \boldsymbol{D_i}\overline{p_i}$. To avoid the overlap, the constraint of local regularization [24] is introduced to penalize the differences of transformations of neighboring vertices by $E_{\text{Regular}} = \sum_i \sum_{j \in \mathcal{N}_i} \left\| (\boldsymbol{D_i} - \boldsymbol{D_j}) \right\|_F^2$. We reconstruct the distance error by adding the weighted constraint of the local regularization as follows:

$$E_{\mathrm{d,R}} = E_{\mathrm{d}} + E_{\mathrm{Regular}} = \sum_i \left\| \boldsymbol{D_i}\overline{p_i} - q_i \right\|^2 + \alpha \sum_i \sum_{j \in \mathcal{N}_i} \left\| (\boldsymbol{D_i} - \boldsymbol{D_j}) \right\|_F^2 \tag{4}$$

where the weight α is set as a constant in this paper.

Minimizing the distance error under the weighted constraint of local regularization can be transferred into solving the linear equations by setting the derivative of the cost function to 0 [24]. The set of deformation transformations is obtained and the template points are transformed into new positions.

In detail, we search for the nearest correspondences on the nominal CAD triangle mesh instead of the nearest mesh vertices when the mesh is not refined enough. In addition, the triangulation for segmented scanned data points can simplify the computation of E_{Regular} by replacing point relations of k-nearest neighbors with the edge of the triangle mesh.

3.3.3 Local rigidity keeping

When projecting the points of the template surface onto the target, shrinking and expanding happen due to the nearest point selection, which is only based on the distance between the selected point and the target surface. In this paper, the interior structure of the surface is introduced, which refers to the relative distance between points and their neighbors. The interior structure of the surface can be used to measure the shrink or expansion of the surface. The shrinking and expanding actually change the interior structure of the segmented scanned data points of the deformed blade. Since only the segmented parts of the nominal CAD and measured data are matched up, the shrink or expansion of these parts should be eliminated as much as possible for the accuracy of the intact deformed blade model. Therefore, keeping the interior structure of these parts, which means the distance relations of vertices and their neighbors, is another main focus in this paper.

To measure the difference of interior structure of the deformed/projected surface, we penalize the changes of position and distance of each defined neighborhood as follows:

$$E_{\mathrm{r}} = \sum_i \sum_{j \in \mathcal{N}_i} \left(\left\| \overrightarrow{p_i p_j} \right\| - \left\| \overrightarrow{p_i' p_j'} \right\| \right)^2 \tag{5}$$

where $p_i' \in \mathbf{P}' = \{p_1', p_2', \ldots, p_N'\}$ is the deformation of $\mathbf{P} = \{p_1, p_2, p_3, \ldots, p_N\}$.

Inspired by the as-rigid-as-possible (ARAP) method [25], we minimize the following local rigidity energy to adjust the interior structure of the deformed template surface

$$\widetilde{E}_{\mathrm{r}} = \sum_i \sum_{j \in \mathcal{N}_i} \omega_{ij} \left\| \left(p_i' - p_j' \right) - \boldsymbol{R_i} \left(p_i - p_j \right) \right\|^2 \tag{6}$$

where ω_{ij} is the cotangent weight on meshes [25] or points cloud [26], and $\boldsymbol{R_i}$ is the optimal rotation for the cell $\left\{ p_i, p_j (j \in \mathcal{N}_i) \right\}$ and its transformed cell $\left\{ p_i', p_j' (j \in \mathcal{N}_i) \right\}$ which can be estimated by singular value decomposition (SVD) [25].

To minimize the local rigidity energy with the given rotations, we set the partial derivatives $\partial \widetilde{E}_{\mathrm{r}} / \partial p_i'$ to be 0 and the following linear equations can be achieved:

$$\sum_{j \in \mathcal{N}_i} \omega_{ij} \left(p_i' - p_j' \right) = \sum_{j \in \mathcal{N}_i} \frac{\omega_{ij}}{2} (\boldsymbol{R_i} + \boldsymbol{R_j}) \left(p_i - p_j \right) \tag{7}$$

The weights ω_{ij} are obtained by the geometry of the original template surface which is the discrete of the Laplace–Beltrami operator. For the segmented scanned points data, the tangent-space optimal weights [26] are adopted and the cotangent weights are used if the segmented scanned data is triangulated into mesh topology before. Rewriting Eq. (7) as $\boldsymbol{L}p' = b$, we obtain the adjusted template data p' through keeping the local rigidity.

In the iteration loop, maximum iterations $i_{\max}$, the threshold of distance error ε_{d}, and the threshold of local rigidity energy ε_{r} are predefined. The iteration will stop when the distance error and local rigidity energy of current template data are all less than the predefined thresholds, or the number of iterations is greater than $i_{\max}$. Figure 6 shows the matched result and comparison result.

3.4 Separation and stitching

We obtain the accurate matching of the corresponding overlap part of the nominal model and the scanned data. According to the matching result and the original position, the rule of deformation about the scanned data is found. However, the matching result is a closely approximated shape of the nominal CAD, not the intact deformed blade model. In this section, 'separation' and 'stitching' are performed to make the nominal model match up with the scanned data on appearance to obtain the deformed blade model for remanufacturing.

Similar to the segmentation we carry out at first, the separation refers to the extraction of the corresponding part of the nominal model for the undamaged part of the SF and PF. The segmented scanned data are embedded in the SF and PF of the nominal model. Since the deposited part has been taken out, the mesh vertices of the nominal model can be recognized and marked as the undamaged part through the matched scanned data. To simplify the following computations, the triangulation for the matched scanned data is carried out firstly. Same as before, we denote by $\boldsymbol{P}' = \{p_1', p_2', \ldots, p_n'\}$ the vertices of matched scanned data whose original data is $\mathbf{P} = \{p_1, p_2, p_3, \ldots, p_n\}$, and by $\mathbf{Q} = \{q_1, q_2, q_3, \ldots, q_m\}$ the vertices of the SF and PF of the nominal model. Because the surfaces of matched scanned data and the segmented nominal model are close enough, we replace the normals of matched scanned data

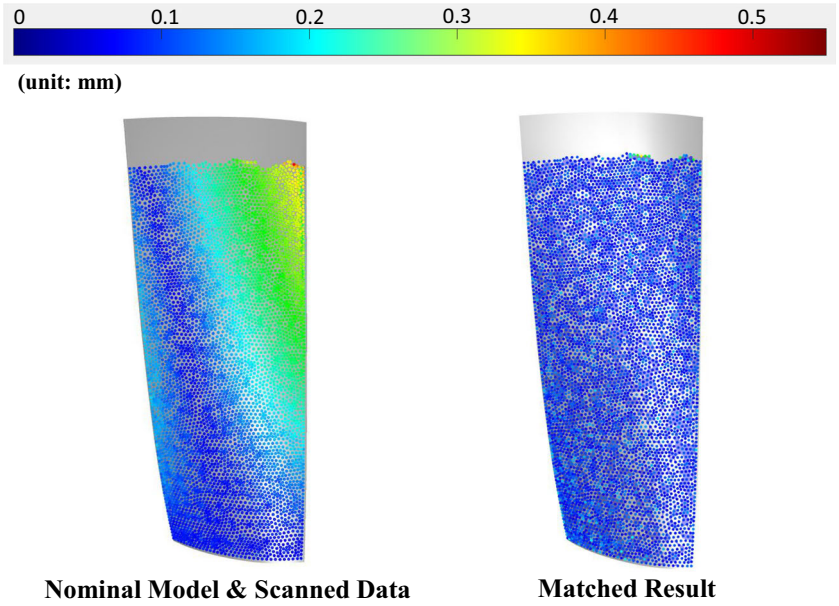

Fig. 6 Matching result analysis and comparison

by those of the nominal model. The vertices of segmented nominal model $\mathbf{Q} = \{q_1, q_2, q_3, \ldots, q_m\}$ are projected onto the surface of matched scanned data along such normals, and the vertices, whose projecting images are in the surface of matched scanned data, are marked as the undamaged part.

Based on the marked vertices, the nominal model is separated into the undamaged part and the rest of the parts. Matching results provide the deformation rule of the segmented scanned data which totally overlap with the undamaged part. To construct an accurate deformed blade model, we firstly make the undamaged part coincide with the scanned data. For each vertex q_i in the undamaged part, the only corresponding triangle $\triangle p_{i1}' p_{i2}' p_{i3}'$ can be found. And q_i has barycentric coordinates $(\alpha_i, \beta_i, \gamma_i)$ which is treated as weights placed at vertices p_{i1}', p_{i2}', p_{i3}'. We get another notation relative to the vertices in the undamaged part with a linear combination of the vertices of the matched scanned data by solving the following linear system:

$$\begin{cases} q_i = \alpha_i \cdot p_{i1}{}' + \beta_i \cdot p_{i2}{}' + \gamma_i \cdot p_{i3}{}' \\ 1 = \alpha_i + \beta_i + \gamma_i \end{cases}, i = 1, \ldots, n \tag{8}$$

These weights are calculated from the relative position of the vertices of the undamaged part and their relative mesh in the matched scanned data. In other words, these weights keep the local rigidity of the matched results. That the weights are kept in the original scanned data makes sense since the local rigidity is kept as much as possible in the matching. To make the undamaged part of the nominal model coincide with the original scanned data, we do not need to compute the reverse transformations for all vertices, but use the one-to-one correspondence between the original scanned data and the transformed one to estimate as follows

$$\begin{aligned} q_i{}' = D^{-1}(q_i) \approx D_{i1}^{-1}\left(\alpha_i \cdot p_{i1}{}'\right) + D_{i2}^{-1}\left(\beta_i \cdot p_{i2}{}'\right) + D_{i3}^{-1}\left(\gamma_i \cdot p_{i3}{}'\right) \\ = \alpha_i \cdot p_{i1} + \beta_i \cdot p_{i2} + \gamma_i \cdot p_{i3} \end{aligned} \tag{9}$$

In the segmentation or separation for the nominal model, the vertices are the objects that we manipulate but the edge relations are not changed which means the mesh topology is also kept. In addition, the vertices on their boundaries q_i $(i \in \mathcal{B})$ caused by the separation are the intersection of the undamaged part and the rest of the parts. Therefore, the undamaged part and the rest of the parts can be stitched together with the vertices on the boundaries caused by the separation to restore an intact model.

The stitching, in essence, is to impose the constraints on these boundary vertices on the deformation of the nominal model. By regarding the edges of the nominal mesh as springs, such deformation should behave like a physical sheet that will stretch or bend when the forces are acting on it. We minimize the local rigidity energy that measures the change of edges' length. Instead of deforming the rest of the parts which may not fit the requirements for surface fairness, we manipulate the two separate parts as a whole by stitching the boundary vertices up to the transformed positions. Similar to Eq. (7), the local rigidity energy of the deformed blade model is defined by

$$\sum_{j \in \mathcal{N}_i} \widetilde{\omega_{ij}} \left(q_i{}' - q_j{}'\right) = \sum_{j \in \mathcal{N}_i} \frac{\widetilde{\omega_{ij}}}{2} \left(\boldsymbol{R_i} + \boldsymbol{R_j}\right) \left(q_i - q_j\right) \tag{10}$$

Equation (10) can be rewritten as $\boldsymbol{L_Q} q' = b_Q$, where L_Q is the discretization of the Laplace–Beltrami operator for the nominal model. Adding the constraints of the fixed boundary vertices $q_i{}'$ $(i \in \mathcal{B})$ into the system, the respective rows and

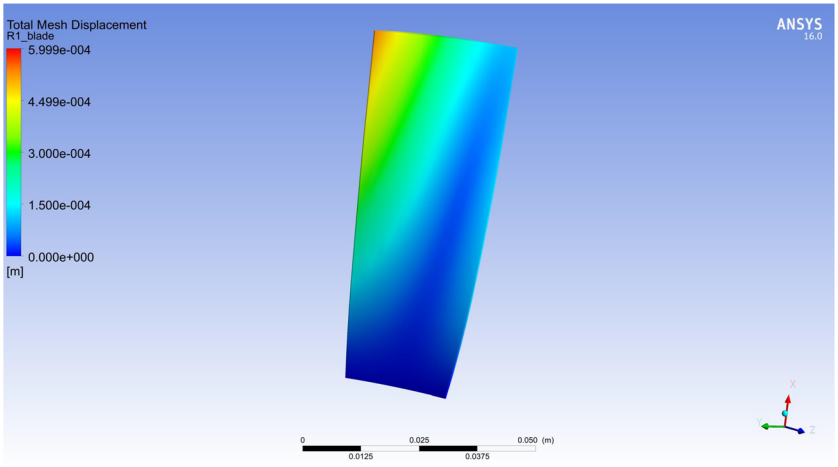

Fig. 7 Standard deformed model from ANSYS CFX

columns in L_Q need to be deleted and b_Q should be updated with these fixed positions $q_i^{'}$ $(i \in \mathcal{B})$. The starting guess about $\mathbf{Q}^{'}$ is obtained by minimizing $\| \boldsymbol{L_Q} q^{'} - \boldsymbol{L_Q} q \|^2$ under the constraints of fixed positions $q_i^{'}$ $(i \in \mathcal{B})$.

4 Results and discussion

The proposed method was applied to the remanufacturing of a twisted compressor blade with the blade tip damage which accords with most cases in blade repairing [27]. The fluid–structure coupling calculation is used to simulate the deformation of the nominal model by the ANSYS CFX as shown in Fig. 7, since working deformation largely reflects the actual blade deformation under high-temperature and pressure working conditions. Therefore, this deformed model from the computational fluid dynamics (CFD) software tool, ANSYS CFX, is regarded as the deformed blade for comparison.

4.1 Simulated input data

As mentioned before, the damaged blade suffers from deformation and being worn. To make the input data as realistic as possible, we simulated the deformed blade data as the deposited blade by adding the welding-like part on the blade tip as shown in Fig. 8. The surface geometry of the deposited blade is scanned and digitized into point clouds by using 3D optical devices. However, the captured points cloud geometry will be limited by the scanning parameters of the specific noncontact device. Setting measuring accuracy as 0.02 mm, the Gaussian noise is adding to the positions of the deposited blade, whose mathematical expectation and variance are 0.02 mm and $(0.02\ \text{mm})^2$, as shown in Fig. 8.

4.2 Deformed blade model construction and comparison

Assuming that the deformed blade also keeps the intrinsic geometry of the new one, we use the nominal model and scanned data of the deposited blade to construct an accurate deformed blade model. Different from the current extrapolation algorithms for blade repairing which only focuses on keeping the C0, C1, or G1 continuity, the proposed method constructs the deformed blade model with the help of the nominal model and the scanned data, and the mesh topology is also kept.

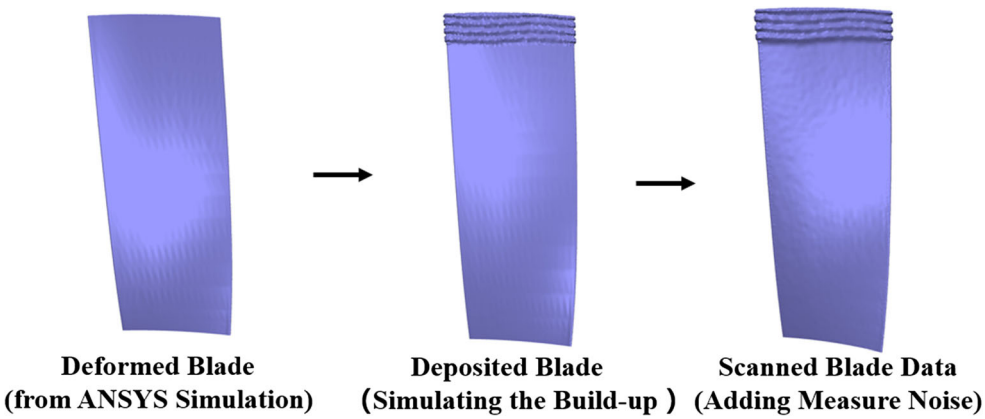

Fig. 8 Input data simulation steps

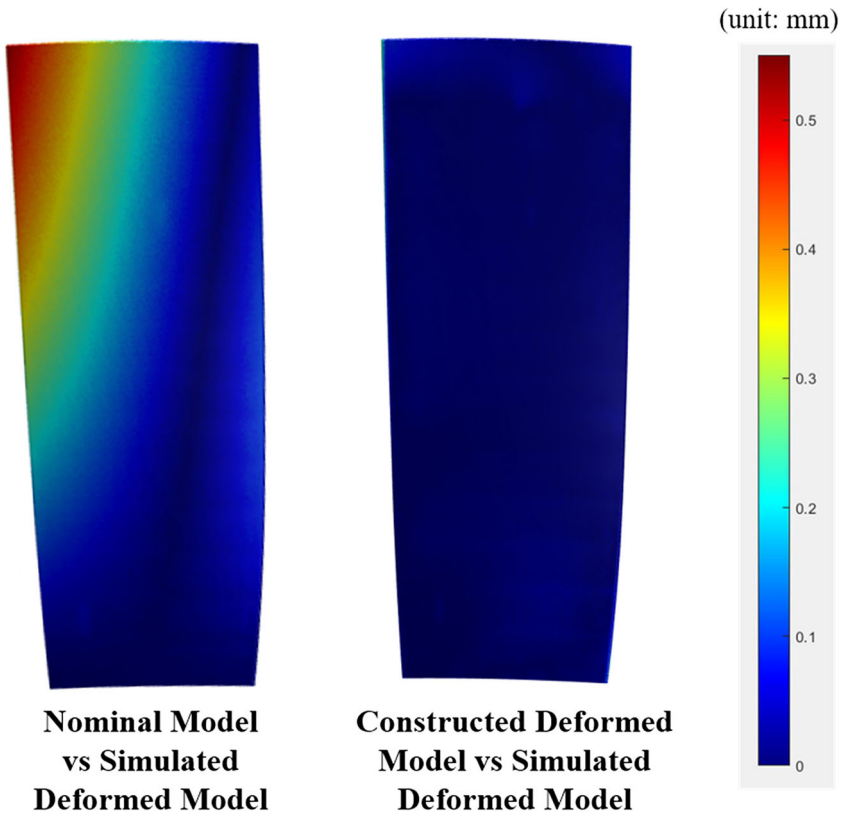

Fig. 9 Constructed deformed model analysis and comparison

To construct the deformed blade model, we firstly match up the scanned data with the nominal model as mentioned in Section 3.3. Figure 6 shows the matching results and the comparison with the previous matching data. Then the vertices of the nominal model are separated and stitched up to their positions of the scanned data to construct the deformed blade model. The deformed blade model is constructed based on the deposited blade scanned data and the nominal model. Moreover, in Fig. 9, the constructed deformed blade model is analyzed and compared with the deformation blade data acquired from the ANSYS CFX to verify the accuracy. The comparison results in Table 1 show that the maximum error of the constructed deformed blade model is 0.06 mm that is the same order of magnitude as the measuring accuracy, and the average error of the constructed deformed blade model is 0.02 mm that is approximated to the mathematical expectation of measuring noises.

In addition, the constructed deformed blade model maintains the same mesh topology as the nominal model. It might be helpful for transferring the machining paths of the nominal model adaptively.

4.3 Simulated machining result

The simulated machining was also carried out to verify the accuracy and reliability of our method. Based on the constructed deformed blade model, the tool paths can be generated to machine the deposited blade. Different from the constructed blade model and the deposited blade, the deposited region was determined and extracted for tool path generation.

The isoparametric machining strategy with the ball-end cutter was adopted. Figure 10 shows the cutter-contact tool paths and cutter-position tool paths. The file of generated tool paths was loaded into CutRight, a machining simulation and verification software developed at UBC, to simulate the machining result and verify our method. The cutting result with scallop height is shown in Fig. 11. Figure 11b and c show that smooth transition occurs at the interface of the cutting part and

Table 1 Deviation analysis result of the constructed deformed model and the nominal model (compare with the standard deformed blade from ANSYS CFX)

	Nominal model	Constructed deformed model
Max error (mm)	0.55	0.06
Average error (mm)	0.12	0.02

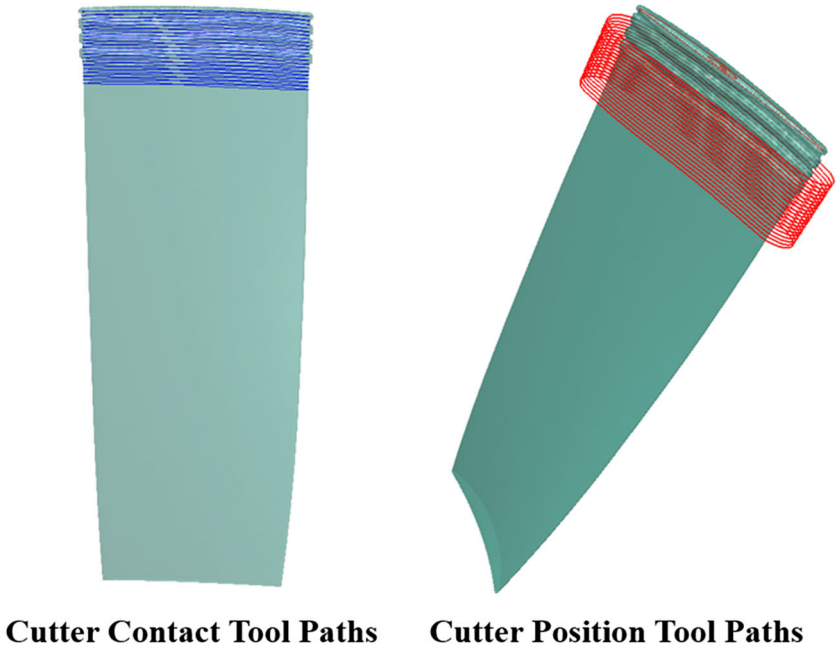

Fig. 10 Simulated blade model and tool path generated on the constructed deformed blade model

the undamaged part which helps to reduce the post-processing time and workload, such as the polishing. Figure 11b shows that the cutting result of the constructed deformed blade model is accurate though a slight overcut still exists. Figure 11d shows the machining result of the top surface of the constructed deformed blade model, which is usually not a plane in the twisted/curved blade and cannot be created easily by the extrapolation operation in the current RE software.

5 Conclusion

Due to the individual geometric variation of deposited/damaged aero-engine blades, it is difficult to construct an accurate model for remanufacturing/repairing automatically. This paper proposed a novel strategy for accurate deformed blade model construction by finding out the relation between the nominal model and the available scanned data. In the segmentation process, the available scanned data was extracted by smoothness

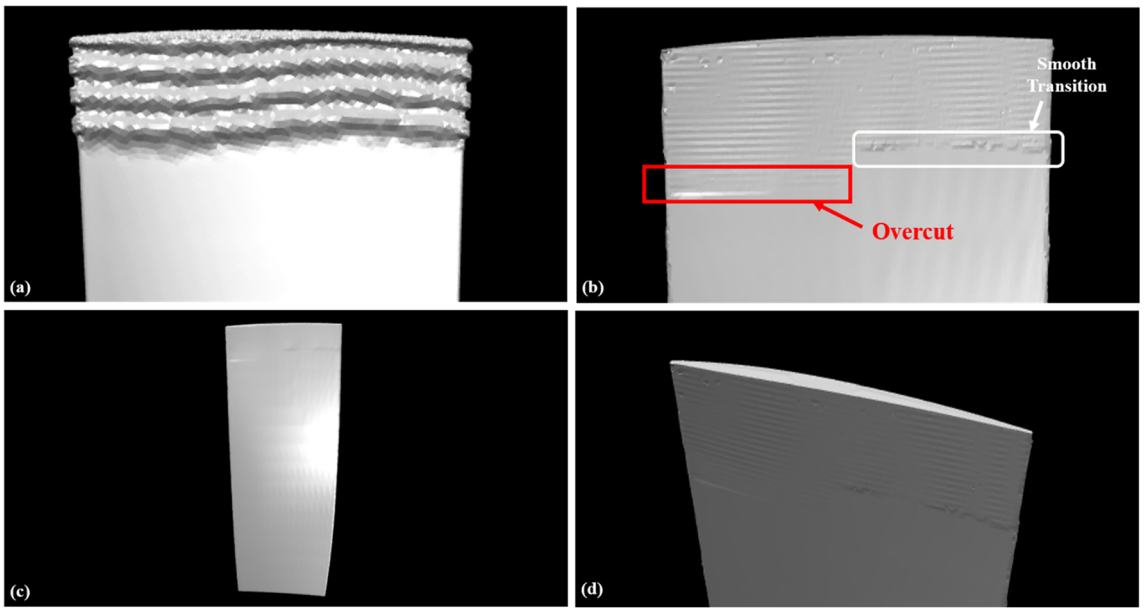

Fig. 11 **a**–**d** Machining simulation result by using CutRight

and curvature. The flattened surfaces of the nominal model, the suction face and the pressure face, were segmented accordingly. The segmented scanned data were matched up with the segmented nominal model by keeping local rigidity as much as possible in the optimal ICP framework. Then the nominal model was stitched up with the scanned data at some selected positions to construct the deformed blade model. Our method was implemented on a twisted compressor blade with tip damage to verify its feasibility. Especially, the deformed standard model acquired by the CFD software tool was utilized to verify the accuracy of the constructed deformed blade model. In addition, the machining simulation result showed the accuracy of the constructed deformed blade model by the smooth transition at the interface which is greatly helpful to reduce post-processing time. Experimental results demonstrated that the proposed method has advantages in geometric accuracy, automation, and repair, saving time for aero-engine blade remanufacturing, especially for twisted/curved blades.

Acknowledgments The authors are thankful to Dr. Jack S.-S. Chen of UBC for his assistance in generating the machining simulation result using CutRight.

Funding information This work has been supported by the National Key Research and Development Program of China (Grant No. 2018YFB1107402) and the National Natural Science Foundation of China (Grant No. 11290141). The support provided by the China Scholarship Council (Grant No. 201706020096) to sponsor the 1-year visit of Cheng Su to the University of British Columbia (UBC) is also gratefully acknowledged.

Compliance with ethical standards

The research does not involve human participants and/or animals. Consent to submit the paper for publication has been received explicitly from all co-authors.

Conflict of interest The authors declare that they have no conflict of interest.

References

1. Antony K C, Goward G W (1988) Aircraft gas turbine blade and vane repair. Superalloys The Metallurgical Society, 745
2. Carter TJ (2005) Common failures in gas turbine blades. Eng Fail Anal 12(2):237–247
3. Gao J, Folkes J, Yilmaz O et al (2005) Investigation of a 3D non-contact measurement based blade repair integration system. Aircr Eng Aerosp Technol 77(1):34–41
4. Gao J, Gindy N, Chen X (2006) An automated GD&T inspection system based on non-contact 3D digitization. Int J Prod Res 44(1): 117–134
5. Brinksmeier E, Berger U, Janssen R (1998) Advanced mechatronic technology for turbine blades maintenance
6. Sheng X, Kromker M (1998) Surface reconstruction and extrapolation from multiple range images for automatic turbine blades repair. IECON'98, Proceedings of the 24th Annual Conference of the IEEE Industrial Electronics Society (Cat. No. 98CH36200), IEEE, 1998, 3: 1315–1320
7. Gandini E, Agnesone F, Taricco F et al (1997) Advances in gas turbine blade repair by laser welding. ASME 1997 International Gas Turbine and Aeroengine Congress and Exhibition. Am Soc Mech Eng V004T12A011-V004T12A011
8. Jones J B, McNutt P, Tosi R, et al (2012) Remanufacture of turbine blades by laser cladding, machining and in-process scanning in a single machine
9. Wilson JM, Piya C, Shin YC et al (2014) Remanufacturing of turbine blades by laser direct deposition with its energy and environmental impact analysis. J Clean Prod 80:170–178
10. Zhang X, Li W, Liou F (2018) Damage detection and reconstruction algorithm in repairing compressor blade by direct metal deposition. Int J Adv Manuf Technol 95(5-8):2393–2404
11. Yilmaz O, Noble D, Gindy NNZ et al (2005) A study of turbomachinery components machining and repairing methodologies. Aircr Eng Aerosp Technol 77(6):455–466
12. Yilmaz O, Gindy N, Gao J (2010) A repair and overhaul methodology for aeroengine components. Robot Comput Integr Manuf 26(2):190–201
13. Bremer C, Kosche T (2006) Automated repair and overhaul system for aero turbine engine components. Aeronautics Days
14. Gao J, Chen X, Yilmaz O et al (2008) An integrated adaptive repair solution for complex aerospace components through geometry reconstruction. Int J Adv Manuf Technol 36(11-12):1170–1179
15. Li L, Li C, Tang Y et al (2017) An integrated approach of reverse engineering aided remanufacturing process for worn components. Robot Comput Integr Manuf 48:39–50
16. Gao J, Chen X, Zheng D et al (2006) Adaptive restoration of complex geometry parts through reverse engineering application. Adv Eng Softw 37(9):592–600
17. Bagci E (2009) Reverse engineering applications for recovery of broken or worn parts and re-manufacturing: three case studies. Adv Eng Softw 40(6):407–418
18. Ng B T J, Lin W J, Chen X, et al (2004) Intelligent system for turbine blade overhaul using robust profile re-construction algorithm. ICARCV 2004 8th Control, Automation, Robotics and Vision Conference, IEEE, 2004, 1: 178–183.
19. Mohaghegh K, Sadeghi MH, Abdullah A (2007) Reverse engineering of turbine blades based on design intent. Int J Adv Manuf Technol 32(9-10):1009–1020
20. Mohaghegh K, Sadeghi MH, Abdullah A et al (2010) Improvement of reverse-engineered turbine blades using construction geometry. Int J Adv Manuf Technol 49(5-8):675–687
21. Rong Y, Xu J, Sun Y (2014) A surface reconstruction strategy based on deformable template for repairing damaged turbine blades. Proc Inst Mech Eng G J Aerosp Eng 228(12):2358–2370
22. Zheng J, Li Z, Chen X (2006) Worn area modeling for automating the repair of turbine blades. Int J Adv Manuf Technol 29(9-10): 1062–1067
23. Tam GKL et al (2013) Registration of 3D point clouds and meshes: a survey from rigid to nonrigid. IEEE Trans Vis Comput Graph 19.7:1199–1217
24. Amberg B, Romdhani S, Vetter T (2007) Optimal step nonrigid ICP algorithms for surface registration. 2007 IEEE Conference on Computer Vision and Pattern Recognition. IEEE 2007:1–8
25. Sorkine O, Alexa M (2007) As-rigid-as-possible surface modeling. Symp Geom Process 4:109–116
26. Schmidt R, Singh K (2009) Approximate conformal parameterization of point-sampled surfaces. University of Toronto Technical Report
27. Compressor blades repair and overhaul (2002) Rolls-Royce Plc Internal Report